Chemical Vapor Deposition of Cu_xS: Surface Contamination by Reaction Products

Liesbeth Reijnen,* Ben Meester, Albert Goossens, and Joop Schoonman

Laboratory for Inorganic Chemistry, Delft University of Technology, Julianalaan 136, 2628 BL Delft, The Netherlands

Received December 5, 2003. Revised Manuscript Received May 3, 2005

Thin films of Cu_xS are grown by chemical vapor deposition using $Cu(thd)_2$ (thd = tetramethylheptanedionate), H_2S, and H_2 as the precursors. A deposition profile, not caused by depletion of the precursors, is present in all films. Hydrogen is needed for growth to occur; in atomic layer deposition of Cu_xS the reaction between $Cu(thd)_2$ and H_2S does not require H_2. To explain these observations, a model is derived on the basis of competitive adsorption of $Cu(thd)_2$ and the reaction product Hthd at the surface. With numerical calculations, the growth rate, the $Cu(thd)_2$ concentration, and the Hthd concentration as a function of the flow axis can be simulated. A deposition profile due to competitive adsorption of $Cu(thd)_2$ and Hthd is found.

Introduction

A new approach to solar cell design is the use of nanostructured heterojunctions of inorganic materials. One of the concepts using this approach is the extremely thin absorber (ETA) solar cell. The ETA solar cell consists of a nanoporous or microporous matrix of a transparent n-type semiconductor and a p-type semiconductor deposited inside the pores. Between the n-type and p-type materials a thin film (e.g., 20 nm) of visible-light-absorbing material is deposited. Up to now TiO_2, among other materials, has been used as the electron conductor, while CdTe[1] and $CuInS_2$[2,3] have been used as inorganic absorber films. In addition to these materials, Cu_2S (chalcocite), with a band gap of 1.2 eV[4] and an absorption coefficient of 10^5 cm^{-1} at 750 nm,[5] is also an interesting absorber and a p-type semiconductor. Furthermore, Cu_2S does not contain poisonous (Cd, Te) or expensive (In) elements.

Cu_xS has five stable phases at room temperature,[6] ranging from Cu_2S to CuS. Besides Cu_2S, $Cu_{1.96}S$ (djurleite) and $Cu_{1.8}S$ (digenite) are also p-type semiconductors. Although both the electrical conductivity and the band gap increase for the Cu-poor phases,[4] they are also suitable for solar energy conversion.

A major challenge in the fabrication of a nanostructured cell is the deposition of the inorganic absorber film (Cu_2S) inside the pores of the n-type semiconductor (TiO_2). Up to now thin films of Cu_xS have been prepared using single-source evaporation,[7−9] (reactive) sputtering,[10,11] and chemical vapor deposition (CVD).[12,13] Among these techniques only CVD is not a line-of-sight technique and can be used for deposition of Cu_2S in a nanoporous matrix. Up to now $[CuCl(NCCH)]_n$,[13] copper(II) bis(acetylacetonate) ($Cu(aa)_2$),[13] methylcopper,[13] and copper(II) bis(diethyldithiocarbonate) ($Cu(dctEt_2)_2$)[12] have been used as precursors. Single-phase Cu_xS films could not be obtained using one of these precursors. β-Diketonates, like $Cu(aa)_2$, copper(II) bis(hexafluoroacetylacetonate) ($Cu(hfac)_2$), and copper(II) bis(tetramethylheptanedionate) ($Cu(thd)_2$) form a group of compounds that are volatile and relatively stable. They have been extensively studied in the CVD of both copper[14] and copper oxide.[15] $Cu(hfac)_2$ readily absorbs water, which might affect the CVD process;[16] $Cu(thd)_2$, however, does not absorb water due to its bulky ligands, making it stable over longer periods of time, even in an ambient gas atmosphere.

Previously, we reported on the atomic layer deposition (ALD) of Cu_xS using $Cu(thd)_2$ and H_2S as the precursors[17] and on the CVD of Cu_xS using $Cu(thd)_2$, H_2S, and H_2 as the precursors.[18] Single-phase films of CuS and of $Cu_{1.8}S$ could

(1) Ernst, K.; Sieber, I.; Neumann-Spallart, M.; Lux-Steiner, M. C.; Könenkamp, R. *Thin Solid Films* **2000**, *361−362*, 213.
(2) Kaiser, I.; Ernst, K.; Fischer, C.-H.; Könenkamp, R.; Rost, C.; Sieber, I.; Lux-Steiner, M. C. *Sol. Energy Mater. Sol. Cells* **2001**, *67*, 89.
(3) Möller, J.; Fischer, C.-H.; Muffler, H.-J.; Könenkamp, R.; Kaiser, I.; Kelch, C.; Lux-Steiner, M. C. *Thin Solid Films* **2000**, *361−362*, 113.
(4) Nair, M. T. S.; Guerrero, L.; Nair, P. K. *Semicond. Sci. Technol.* **1998**, *13*, 1164.
(5) Hewig, G. H.; Pfisterer, F.; Schock, H. W.; Arndt, W.; Bloss, W. H. *Conf. Rec. IEEE Photovoltaic Spec. Conf.* **1982**, *16*, 713.
(6) Hwang, H. L.; Loferski, J. J.; DeMeo, E. A.; Beaulieu, R. *J. Cryst. Growth* **1982**, *59*, 425.
(7) Llabres, J.; Arjona, F. *Phys. Status Solidi A* **1980**, *58*, 153.
(8) Aperathitis, E.; Bryant, F. J.; Scott, C. G. *Sol. Energy Mater.* **1990**, *20*, 15.
(9) Leon, M.; Terao, N.; Rueda, F. *J. Mater. Sci.* **1984**, *19*, 113.
(10) Iborra, E.; Santamaria, J.; Martil, I.; Gonzalez-Diaz, G.; Sanchez-Quesada, F. *Vacuum* **187**, *37*, 437.
(11) Vanhoecke, E.; Burgelman, M.; Anaf, L. *Thin Solid Films* **1984**, *144*, 233.
(12) Nomura, R.; Miyawaki, K.; Toyosaki, T.; Matsuda, H. *Chem. Vap. Deposition* **1996**, *2*, 174.
(13) Hwang, H. L.; Ho, J. S.; Ou, H. J.; Lee, Y. K.; Sun, C. Y.; Chen, C. J.; Loferski, J. J. *Conf. Rec. IEEE Photovoltaic Spec. Conf.* **1981**, *15*, 1035.
(14) Bakovets, V. V.; Levashova, T. M.; Dolgovesova, I. P.; Danilovich, V. S. *Inorg. Mater.* **2002**, *38*, 457.
(15) Klippe, L.; Wahl, G. *J. Alloys Compd.* **1997**, *251*, 249.
(16) Mårtenson, P.; Carlsson, J.-O. *J. Electrochem. Soc.* **1998**, *145*, 2926.
(17) Reijnen, L.; Meester, B.; Goossens, A.; Schoonman, J. *Chem. Vap. Deposition* **2003**, *9*, 15.
(18) Reijnen, L.; Meester, B.; Goossens, A.; Schoonman, J. *Chem. Mater.*, in press.

10.1021/cm035276v CCC: $30.25
Published on Web 07/09/2005

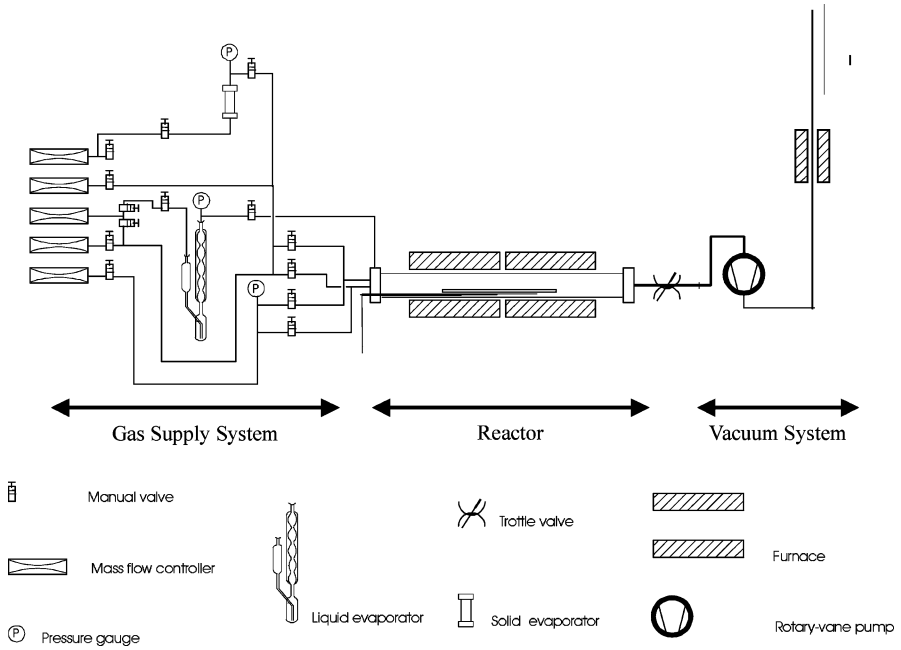

Figure 1. Schematic presentation of the CVD equipment.

be obtained with both processes. In these studies we showed that the temperature dependence of the obtained crystalline phases and the morphology obtained by CVD can be explained by comparing the CVD and ALD processes and by studying the decomposition of $Cu(thd)_2$. In addition it was found that a deposition profile is present in films grown by CVD and deposited with widely varying deposition parameters. The occurrence of this deposition profile is detrimental to the construction of an ETA cell due to the uncontrolled growth rate, making deposition in the pores of TiO_2 difficult. The present investigations show that depletion of reactants is not responsible for the deposition profile. Instead, contamination by Hthd, being a volatile reaction product, occurs. Indeed, a model based on competitive occupation of reaction sites can explain the experimental findings.

Experimental Aspects

Cu_xS films are deposited with a home-built LP-CVD reactor, which is schematically presented in Figure 1. The system can be divided into three sections, i.e., the reactor, the gas supply system, and the vacuum system. The reactor consists of a 50 mm i.d. quartz tube of 600 mm length in a horizontal resistance-heated two-zone furnace, with zones of 290 mm each. A glass substrate holder of 300 mm length is positioned in the middle of the reactor. The temperature is measured in the middle of the reactor and at 75 mm to both ends by three Ni/CrNi thermocouples. Small temperature variations along the flow axis exist. The temperature difference between the middle of the reactor and 75 mm to either side of the middle is 5 °C at 300 °C and 8 °C at 350 °C. All reactor temperatures given in this paper are those in the middle of the reactor. The gas supply system consists of one line for the carrier gas for $Cu(thd)_2$ (Aldrich), one line for H_2S (4.8 hoekloos), and two lines for the bulk gases. Hydrogen (4.8 hoekloos) is used as the carrier and bulk gas in most experiments, while in a limited number of experiments argon (4.8 hoekloos) is used as the bulk and carrier gas. Mass flow controllers (Bronkhorst Hitec) control all carrier, precursor, and bulk flows. $Cu(thd)_2$ is evaporated in a quartz boat placed inside the reactor at 117 °C. An additional quartz tube of 6 mm i.d., enveloping the quartz boat, prevents H_2S from reacting with the $Cu(thd)_2$ powder (see Figure 2). A 4 m^3/h dual-stage rotary-vane pump (Leybold D4B) maintains low pressure, and a diaphragm gauge (MKS Baratron type 122A) regulates the pressure inside the reactor.

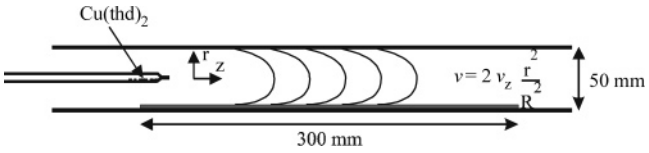

Figure 2. Schematic presentation of the reactor tube. $Cu(thd)_2$ is evaporated from the small tube, which has an exit diameter of 2 mm. The sample holder (gray) is shifted 4 cm under the evaporation tube. $r = 0$ in the middle of the reactor, and $z = 0$ at the exit of the evaporation tube. The gas-velocity distribution profile[19] is given in which v is the velocity as a function of r (m/s), v_z is the average velocity in the z-direction (m/s), and R is the radius of the tube (25 mm).

Glass microscope slides (Menzel-Glaser) and TiO_2 (deposited by CVD in our laboratory) are used as substrates. They are cleaned ultrasonically in 1:1:1 ethanol, methanol, and propanol, subsequently rinsed in distilled water, and dried under a N_2 flow.

The film thickness of the deposited Cu_xS films is measured using a surface texture profiler (Dektak 3030ST), while grazing incidence X-ray diffraction (XRD) measurements (Bruker D8 Advance diffractometer) have been carried out to identify the crystalline phases. The program gPROMS (Process Systems Enterprise) is used to perform the numerical simulations.

Results

Thin films of Cu_xS can be deposited between 125 and 505 °C using $Cu(thd)_2$, H_2S, and H_2 as the precursors. The crystalline phase is strongly dependent on the temperature. Roughly five temperature regimes can be distinguished. Single-phase CuS is grown up to 227 °C. Above this temperature $Cu_{1.8}S$ appears in the films. The $Cu_{1.8}S$ fraction increases with increasing temperature, and at 284 °C single-phase $Cu_{1.8}S$ is formed. Increasing the temperature above 314 °C yields the formation of fractions of $Cu_{1.96}S$ and Cu_2S

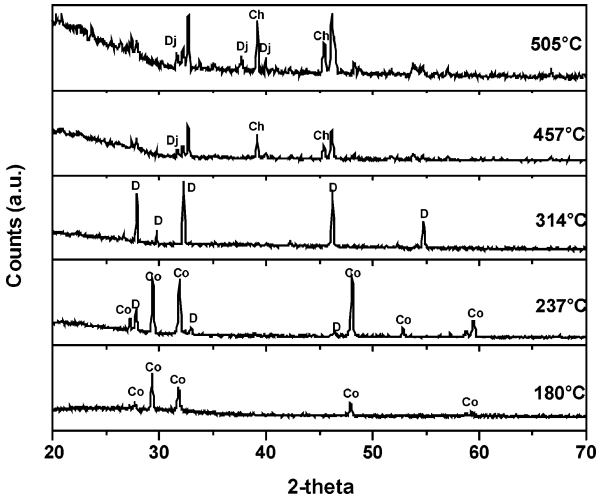

Figure 3. XRD patterns of CVD-grown films: Co, CuS (covelitte); D, $Cu_{1.8}S$ (digenite); Dj, $Cu_{1.96}S$ (djurleite); Ch, Cu_2S (chalcocite).

Table 1. Dependence of the Crystalline Phases on the Deposition Temperature

temp (°C)	crystalline phase	name
125−227	CuS	covellite
227−284	CuS, $Cu_{1.8}S$	covellite, digenite
284−340	$Cu_{1.8}S$	digenite
340−460	$Cu_{1.8}S$, $Cu_{1.96}S$	digenite, djurleite
460−505	$Cu_{1.8}S$, $Cu_{1.96}S$, Cu_2S	digenite, djurleite, chalcocite

in the films (see Table 1 and Figure 3). The morphology of CVD films depends strongly on the deposition temperature as well. Between 125 and 248 °C well-adhering films are deposited. The size of the grains increases with increasing temperature from an average of 0.36 μm at 175 °C to an average of 1.15 μm at 248 °C. Increasing the deposition temperature beyond 250 °C results in the deposition of rough films with different grain sizes randomly distributed across the surface (see Figure 4). This implies a shift in the CVD process from a reaction-limited regime to a thermodynamic regime at 250 °C.

A pronounced deposition profile, which increases with increasing temperature, is present in all films as illustrated in Figure 5. Above 250 °C the films become too rough for an accurate determination of the growth rate, but the same general deposition profile is present. Investigation of the deposition profile is meaningless in the thermodynamic regime because reactions take place in the gas phase. Therefore, we investigate the deposition profile only at temperatures below 250 °C.

Influence of $Cu(thd)_2$ Partial Pressure. In CVD the presence of a deposition profile along the flow axis is usually due to depletion of one or more of the precursors. In this case, however, only 0.0088% of the $Cu(thd)_2$ and only 0.073% of the H_2S in the gas phase are consumed in the reactor at 175 °C, with partial pressures of 2 and 0.24 mbar of $Cu(thd)_2$ and H_2S, respectively.

Even though depletion is highly unlikely, the $Cu(thd)_2$ partial pressure has been varied to exclude this possibility beyond doubt. Figure 6 shows the growth rate and profile as a function of the $Cu(thd)_2$ partial pressure at 175 °C; experiments at 200 and 225 °C show the same behavior. The maximum growth rate increases with increasing $Cu(thd)_2$ partial pressure, and the maximum shifts downstream in the reactor. Yet a pronounced growth rate profile remains for $Cu(thd)_2$ partial pressures as high as 21 mbar, indicating that depletion of $Cu(thd)_2$ is not causing the thickness profile.

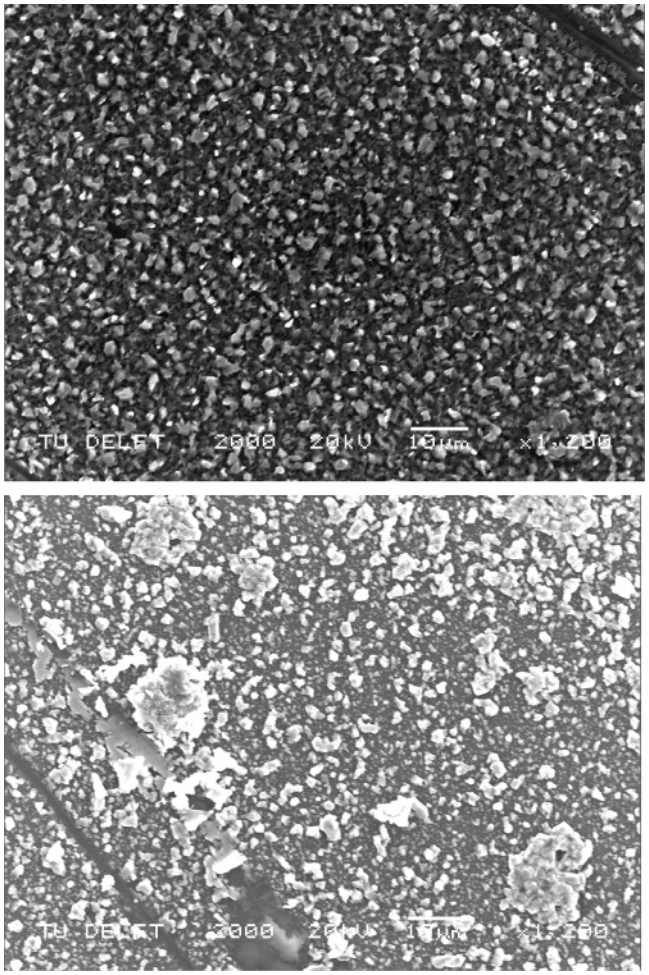

Figure 4. Surface morphology of a smooth CVD-grown $CuS/Cu_{1.8}S$ film deposited at 248 °C (A, top) and of a rough Cu_xS film deposited at 505 °C (B, bottom) as determined by scanning electron microscopy (SEM).

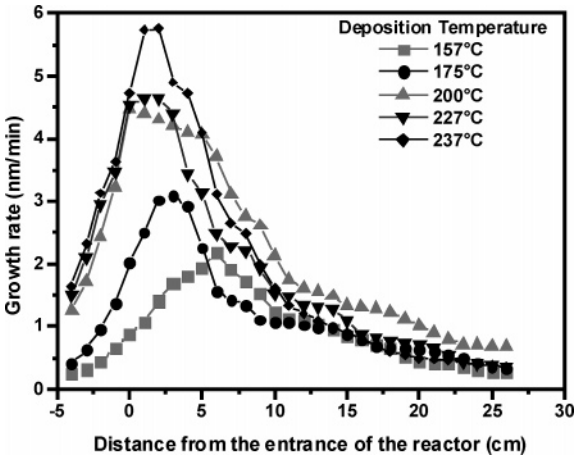

Figure 5. Influence of temperature on the growth rate and deposition profile. Zero on the *x*-axis marks the exit of the $Cu(thd)_2$ evaporation tube.

Influence of the H_2 Partial Pressure. Hydrogen is used as both the carrier and bulk gas, and its partial pressure of 25 mbar is high compared to those of $Cu(thd)_2$ and H_2S. Remarkably, growth is fully inhibited when hydrogen is replaced by argon. When small partial pressures of hydrogen

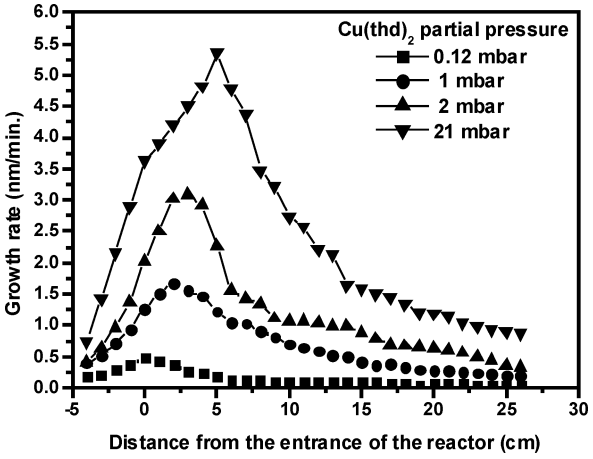

Figure 6. Influence of $Cu(thd)_2$ partial pressure on the growth rate and deposition profile. Zero on the *x*-axis marks the exit of the $Cu(thd)_2$ evaporation tube.

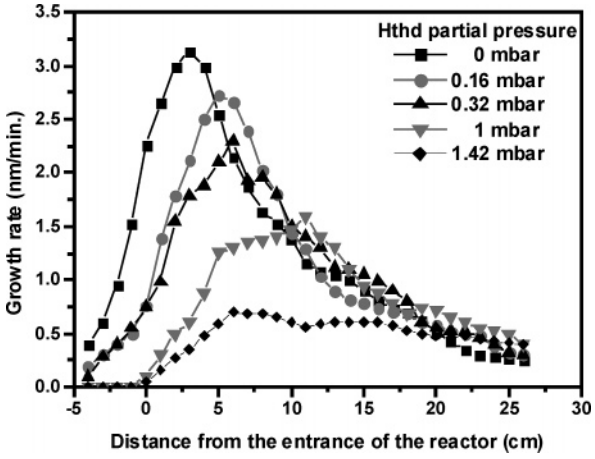

Figure 7. Influence of an additional partial pressure of Hthd on the growth rate and deposition profile. Zero on the *x*-axis marks the exit of the $Cu(thd)_2$ evaporation tube.

are added to the gas stream at 175 °C, the growth rate increases. Up to a H_2 partial pressure of 1 mbar, the thickness profile is almost uniform and the growth rate is about 0.5 nm/min. At higher partial pressures of H_2, the thickness profile becomes more pronounced and again the thickest films appear near the entrance of the reactor. At a H_2 partial pressure of 5 mbar, the growth rate at the start of the deposition zone saturates at 3 nm/min.

Although hydrogen is needed for CVD growth of Cu_xS, this is not the case in ALD of Cu_xS, which shows that the reaction between $Cu(thd)_2$ and H_2S occurs without the presence of H_2. Therefore, another reaction mechanism, not occurring in the ALD of Cu_xS but essential to the CVD of Cu_xS, consumes H_2.

It has been shown previously that side reactions can influence the CVD process. Bloem and Giling[19] have shown that CVD growth of silicon from SiH_2Cl_2 or $SiCl_4$ and H_2 is limited by etching of Si by the reaction product HCl. Others, like Maruizume et al.,[20] have shown that competitive adsorption of the precursor and reaction product limits the conformity of films deposited in trenches. Finally, CO is known to limit the growth rate by blocking active surface sides for precursor molecules.[21] Cohen et al.[22] have shown that the thd ligand adsorbs at metallic surfaces and can only be removed by a reducing agent such as H_2. Haukka et al.[23] report that Hthd adsorbs at OH groups at an oxide surface. We, therefore, propose that the Hthd, which is released as reaction product in the reaction between $Cu(thd)_2$ and H_2S, adsorbs on the surface predominantly at SH groups and can only be removed by hydrogen. When hydrogen is absent, the adsorbed thd ligand cannot be removed from the surface and will permanently block the surface sides for $Cu(thd)_2$, which terminates the growth process. When H_2 is added, Hthd is removed from the surface and the Cu_xS growth rate increases. At a partial pressure of 5 mbar enough H_2 is present to remove all thd ligands from the surface. A competitive adsorption between $Cu(thd)_2$ and Hthd then exists. Because $Cu(thd)_2$ is consumed in the reaction and Hthd is produced, the $Cu(thd)_2$/Hthd ratio will decrease along the flow axis. This leads to a reduction of the growth rate in the same direction and hence the thickness profile.

Influence of the Hthd Partial Pressure. To verify whether Hthd is responsible for the deposition profile, a small amount of Hthd is added to the gas phase. Figure 7 shows the growth rate and thickness profile as a function of the Hthd partial pressure at a deposition temperature of 175 °C and $Cu(thd)_2$ and H_2S partial pressures of 2 and 0.24 mbar, respectively. Clearly, the maximum growth rate decreases with increasing Hthd partial pressure and the maximum growth rate shifts downstream in the reactor. Also the growth profile becomes less pronounced if the Hthd partial pressure is increased. The decreasing maximum growth rate proves that the presence of Hthd in the gas phase limits the growth rate. Because the maximum growth rate decreases, the production of Hthd decreases as well. The Hthd/$Cu(thd)_2$ ratio will increase to a lesser extent along the flow axis with higher Hthd partial pressure, and the deposition profile will become less pronounced.

Model. A model for the deposition of Cu_xS using $Cu(thd)_2$ and H_2S can be designed on the basis of the above assumptions. To simplify the reaction equations, we choose the growth of single-phase CuS, which occurs at temperatures between 125 and 227 °C, but the model can be expanded to include the reaction mechanisms that occur at other temperatures.

The first step is the adsorption of $Cu(thd)_2$ on the surface. We have shown previously[17,18] that a deposition profile is expected in the ALD of Cu_xS when $Cu(thd)_2$ decomposes during adsorption at the substrate surface. The absence of such a profile indicates that $Cu(thd)_2$ adsorbs at the surface without decomposition:

$$Cu(thd)_2(g) + s \xrightarrow{k_A} Cu(thd)_2(ad) \qquad (R1)$$

in which "s" denotes an active surface site. Subsequently,

(19) Bloem, J.; Giling, L. J. *VLSI Electron.: Microstruct. Sci.* **1985**, *12*, 89.
(20) Maruizume, T.; Ushio, J.; Takemura, Y.; Kobayashi, N. *Proc.—Electrochem. Soc.* **1997**, *97-25*, 115.
(21) Carlton, H. E.; Goldberger, W. M. *J. Met.* **1965**, *17*, 611.
(22) Cohen, S. L.; Liehr, M.; Kasi, S. *Appl. Phys. Lett.* **1992**, *60*, 50.
(23) Haukka, S.; Lindblad, M.; Suntola, T. *Appl. Surf. Sci.* **1997**, *112*, 23.

an exchange reaction takes place between the adsorbed $Cu(thd)_2$ and the H_2S in the gas phase:

$$Cu(thd)_2(ad) + H_2S(g) \xrightarrow{k_R} CuS(s) + 2Hthd(g) \quad (R2)$$

The reaction product Hthd adsorbs competitively according to

$$2Hthd(g) + 2s \xrightarrow{k_{Hthd}} 2thd(ad) + H_2(g) \quad (R3)$$

As argued above the thd ligand adsorbed at the surface can be removed by H_2 by the reverse reaction R3.

Reaction models in CVD are usually based on the Langmuir−Hinselwood (L−H) or the Eley−Rideal (E−R) model. In these models it is assumed that all surface sites are thermodynamically and kinetically identical and that the surface coverage of adspecies does not influence the adsorption behavior. Moreover, all reactions are supposed to be in equilibrium except for the rate-determining step (rds), which in this case is reaction R2. In L−H models the reactant species adsorb competitively at the surface, while in E−R models one or more reactant species adsorb at the surface and subsequently react with reactant species in the gas phase. The model described above is an E−R model, and the growth rate is derived:

$$r = \frac{k_R K_A P_{Cu(thd)_2} P_{H_2} S}{1 + K_A P_{Cu(thd)_2} + \dfrac{K_{Hthd}^{1/2} P_{Hthd}}{P_{H_2}^{1/2}}} \quad (E1)$$

in which r is the reaction rate, k_R is the reaction rate constant of reaction R2, K_A and K_{thd} are the equilibrium constants of reactions R1 and R3, respectively, and $P_{Cu(thd)_2}$, P_{H_2S}, P_{Hthd}, and P_{H_2} are the partial pressures of $Cu(thd)_2$, H_2S, Hthd, and H_2, respectively.

To show that a thickness profile can indeed be explained by competitive adsorption between $Cu(thd)_2$ and Hthd, the growth rate is calculated as a function of the flow axis using eq E1 for the growth rate in combination with the concentrations of $Cu(thd)_2$ and Hthd at every point in the reactor. A schematic view of the reactor including dimensions is shown in Figure 2. Two mechanisms are responsible for transport of species in the reactor: convection in the z-direction and diffusion in both the z- and the r-directions. The flux in the z-direction is governed by forced convection, resulting in laminar flow; the diffusion component is negligible in comparison to the forced convection. The forced convection component of the flux is

$$j_z = v(r)C \quad (E2)$$

in which j_z is the molar flux caused by convection, v is the gas velocity, and C is the concentration of the species concerned. The gas velocity v is a parabolic distribution dependent on r as shown in Figure 2. The flux in the r-direction is caused solely by diffusion, and Fick's law applies, i.e.

$$j_r = -D\frac{\delta C}{\delta r} \quad (E3)$$

in which j_r is the flux in the r-direction caused by diffusion, D is the binary diffusion coefficient of the species concerned in H_2, and C is the concentration of the species concerned. The binary diffusion coefficient is defined as the diffusion coefficient of species A in a fluid medium of species B.[24] The binary diffusion coefficients of both $Cu(thd)_2$ and Hthd in H_2 are not known and have been calculated using the model based on diffusion volume increments as derived by Fuller et al.[24] Although the diffusion volume of copper is not known, the diffusion volumes of the other elements in $Cu(thd)_2$ are and the large volume and mass of the thd ligand ensure that only a small error in the calculated diffusion coefficient is introduced. The diffusion coefficient then becomes 4.67 cm^2/s for $Cu(thd)_2$ and 6.5 cm^2/s for Hthd.

Using eqs R2 and R3 and taking the cylindrical shape of the reactor tube into account, we obtain

$$\frac{\delta C}{\delta t} = D\left(\frac{2}{r}\frac{\delta C}{\delta r} + \frac{\delta^2 C}{\delta r^2}\right) - v(r)r\frac{\delta C}{\delta z} \quad (R4)$$

The following initial and boundary conditions apply. First, a steady-state situation ($\delta C/\delta t = 0$) exists in the reactor. Second, at the entrance of the reactor ($z = 0$), we assume that no growth has occurred yet and the precursor concentrations are the supplied concentrations, i.e., $[Cu(thd)_2] = 0.0536$ mol/m^3 (corresponding to a partial pressure of 2 mbar at 175 °C), $[H_2S] = 2.6 \times 10^{-3}$ mol/m^3 (corresponding to a partial pressure of 0.24 mbar at 175 °C), and [Hthd] = 0 mol/m^3. Third, at the reactor tube radius ($r = 25$ mm) film growth takes place. The flux $j_{r,Cu(thd)_2}$ can be described by eq E1, in which the partial pressures have been replaced by actual concentrations. The flux $j_{r,Hthd}$ is dependent on the flux $j_{r,Cu(thd)_2}$ according to reaction R3, i.e., $j_{r,Hthd} = -2j_{r,Cu(thd)_2}$.

Figure 2 shows that $Cu(thd)_2$ is supplied into the reactor using a tube with a small outlet diameter of 2 mm. This small outlet, in combination with the relatively high flow of carrier gas over the $Cu(thd)_2$ powder, ensures that H_2S cannot diffuse back and react with the $Cu(thd)_2$ powder before it has evaporated. This implies that the $Cu(thd)_2$ distribution through the plane at $z = 0$ is not uniform and entrance effects will be observed; e.g., there is growth at $z = 0$ due to diffusion in the opposite direction of the forced flow (see Figures 5−7). In addition, a velocity entrance length z_v can be defined as the length that is needed for the parabolic velocity profile to develop inside a circular tube. This velocity entrance length is given by $z_v = 0.035D(Re)$ in which D is the diameter of the tube and Re is the Reynolds number (Dv/η, with D the diameter of the tube, v the average gas velocity, and η the gas viscosity).[25] In our case z_v is typically around 3 cm for low temperatures and low $Cu(thd)_2$ partial pressures. Figures 5 and 6 show that this theoretical z_v corresponds closely to the position of the maximum growth rate with respect to the entrance of the reactor. Because these entrance effects have been neglected

(24) Fuller, E. N.; Schettler, P. D.; Giddings, J. C. *Ind. Eng. Chem.* **1966**, *58*, 19.

(25) Poirier, D. H.; Geiger, G. H. *Transport Phenomena in Materials Processing*; The Minerals, Metals & Materials Society: Warrendale, PA, 1994.

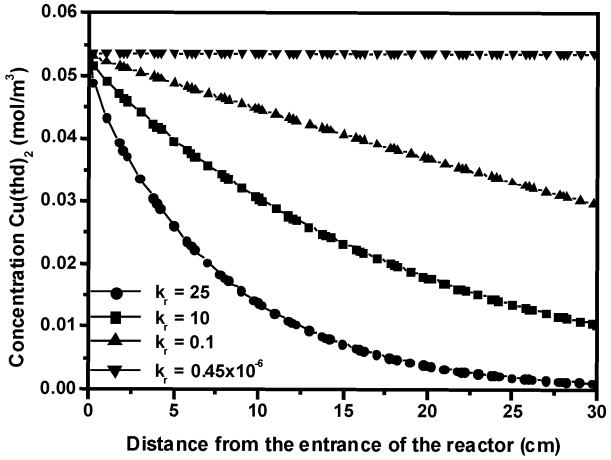

Figure 8. Calculation of the influence of k_R on the $Cu(thd)_2$ concentration profile ($K_A = 0.1$, $K_{Hthd} = 0$).

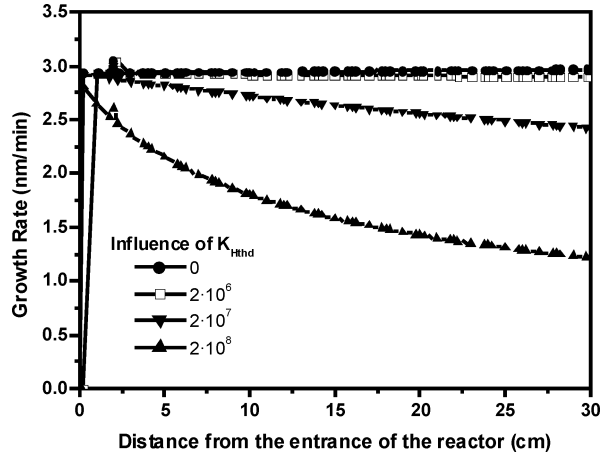

Figure 9. Calculation of the influence of K_{Hthd} on growth rate ($K_A = 0.1$, $K_R = 0.45 \times 10^{-6}$).

in our model, we cannot simulate the increase in growth rate near the entrance of the reactor.

Numerical Simulations. With the above model the Hthd concentration distribution and the growth rate are calculated for different values of k_r, K_A, and K_{Hthd}. Figure 8 shows the $Cu(thd)_2$ concentration as a function of the flow axis at different k_r values. If a realistic value for k_r is chosen, e.g., 0.45×10^{-6}, the $Cu(thd)_2$ concentration is constant throughout the reactor and, as expected, depletion of $Cu(thd)_2$ is not an issue. The calculated growth rates at this k_r value are of the same order of magnitude as the measured growth rates, i.e., 1−3 nm/min, as can be seen in Figure 9. To show that a deposition profile due to depletion of $Cu(thd)_2$ can be simulated using the present model, the value of k_r is increased. This results in an increase of the rate of the reaction between $Cu(thd)_2$ and H_2S and thus in an increase of the calculated growth rate and the $Cu(thd)_2$ consumption. Figure 8 shows that depletion of $Cu(thd)_2$ occurs at values of k_r of 0.1, 10, and 25. The corresponding growth rates and deposition profiles are shown in Figure 10. It is evident that for these unrealistically high values of k_R a deposition profile due to depletion of $Cu(thd)_2$ is present, but the high values of k_r that are needed to simulate depletion of $Cu(thd)_2$ result in an unrealistically high growth, i.e., on the order of 10−70 cm/min.

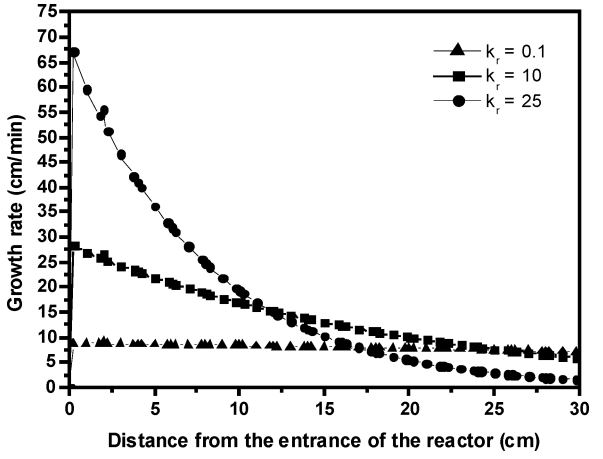

Figure 10. Calculated growth rate as a function of z for different k_R values ($K_A = 0.1$, $K_{Hthd} = 0$).

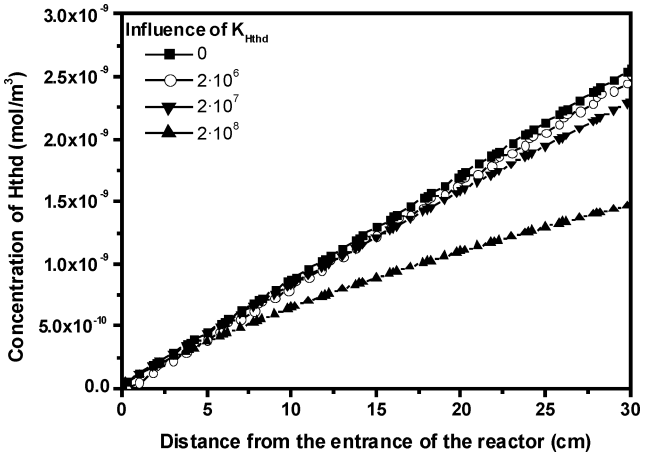

Figure 11. Calculated Hthd concentration as a function of z for different K_{Hthd} values ($K_A = 0.1$, $k_r = 0.45 \times 10^{-6}$).

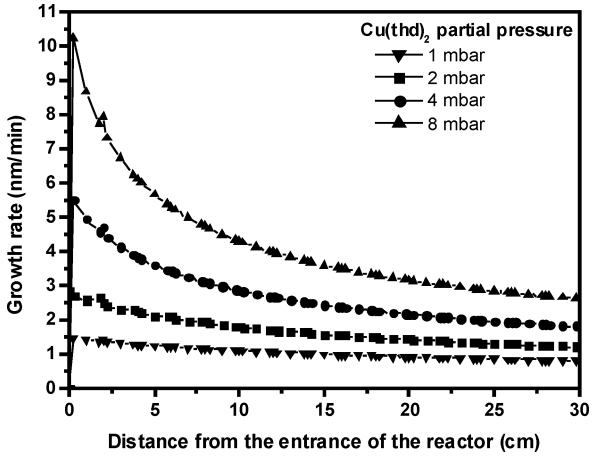

Figure 12. Calculation of the influence of $Cu(thd)_2$ partial pressure on the growth rate as a function of z ($K_A = 0.1$, $k_r = 0.45 \times 10^{-6}$, $K_{Hthd} = 2 \times 10^8$).

Figure 9 shows the growth rate and deposition profile as a function of K_{Hthd}. When K_{Hthd} is 0, we assume that Hthd does not adsorb at the surface and in this case a deposition profile is absent. When K_{Hthd} is increased, a deposition profile starts to appear, indicating that Hthd does adsorb at the surface and interferes with the adsorption of $Cu(thd)_2$. Figure 11 shows the Hthd concentration as a function of the flow axis, which increases monotonically, as expected. The

increase in Hthd concentration becomes less for higher K_{Hthd} values, due to the decreasing growth rate and hence a lower Hthd production.

The growth rate as a function of the $Cu(thd)_2$ partial pressure is shown in Figure 12. In accordance with Figure 6 the deposition profile becomes more pronounced with increasing $Cu(thd)_2$ partial pressure, and also the maximum growth rates for a $Cu(thd)_2$ partial pressure of 1 and 2 mbar are in accordance with those found in Figure 6. The model becomes less accurate at higher $Cu(thd)_2$ partial pressures, because the binary diffusion coefficients as calculated for both $Cu(thd)_2$ and Hthd only apply to diluted systems.

The value of K_{Hthd} at which the deposition profile starts to appear is fairly high, meaning that the adsorption reaction of Hthd is practically irreversible. This is in correspondence with the experimental findings, where the partial pressure of H_2 needs to be very high as opposed to the partial pressure of Hthd for significant growth to occur.

Conclusions

The presence of a deposition profile and the necessity for additional H_2 in the CVD of Cu_xS films using $Cu(thd)_2$ and H_2S as the precursors can be adequately explained by competitive adsorption of the precursor $Cu(thd)_2$ and the reaction product Hthd. The Hthd that is formed in the reaction between $Cu(thd)_2$ and H_2S adsorbs at the surface, releasing H_2 and thus blocking adsorption sides for $Cu(thd)_2$. This adsorbed Hthd can only be removed by H_2. The numerical calculations show that the concentration of Hthd and hence its adsorption increase along the flow axis and that this increase in concentration is responsible for the deposition profile. Although the model explains the experimental findings perfectly, more experimental data are needed to refine the model and to obtain accurate quantitative values for the parameters k_r, K_A, and K_{Hthd}.

CM035276V